Azerbaijani Astronomical Journal AAJ **20(2)**, 28–35 (2025) Preprint 4 December 2025 https://doi.org/10.59849/2078-4163.2025.2.28

SPECTRAL AND PHOTOMETRICAL PROPERTIES OF SELECTED MASSIVE HERBIG AeBe STARS

F. S. Huseynova[1*], N. Z. Ismailov[2], U. S. Veliyev[1]

[1] *Batabat Astrophysical Observatory, Nakhchivan State University, Nakhchivan*
[2] *Tusi Shamakhy Astrophysical Observatory, Ministry of Science and Education of Azerbaijan, Shamakhy*

Last updated 2025 October 19; in original form 2025 November 28

ABSTRACT

This paper presents the results of spectral and photometric studies of six selected massive Herbig Ae/Be stars conducted during 2023–2024. Spectral observations reveal significant variability in the emission-line spectra over time intervals ranging from one month to one year. Spectral energy distributions (SEDs) were constructed to characterize the state of the circumstellar disks. Our analysis shows that two of the six stars possess evolved debris disks with weak residual dust emission. The fundamental physical parameters of the stars were calculated, and their evolutionary status was determined. MWC 300 appears to be a more evolved system exhibiting strong excess infrared radiation, which is likely related to its binary nature.

Key words: stars: pre-main sequence stars, massive HAeBe stars, circumstellar disks, evolution state

1 INTRODUCTION

Herbig AeBe stars (HAeBe), as a group of stars with common physical characteristics, were first identified in the work of Herbig (1960). By that time, a group of T Tauri stars (TTS) was known low-mass ($0.5\leqslant M_*/M_\odot \leqslant 2.0$) stars with emission lines in the spectrum. HAeBe stars are now believed to have intermediate masses of $2.0\leqslant M_*/M_\odot \leqslant 10$, and have the same physical properties as TTS. HAeBe stars have emission and absorption lines in the spectrum, typical spectral types A-B, are located in dark gas and dust nebulae, have excess radiation in the infrared (IR) part of the spectrum Finkenzeller and Mundt (1984); Herbig and Bell (1988); The et al. (1994); Carmona et al. (2010); Chen et al. (2016).

To date, more than 300 HAeBe type stars are known Guzmán-Díaz et al. (2021). This is much smaller than the thousands of known TTSs, and this discrepancy can be partly explained by the shape of the initial mass function (IMF), which favors the formation of less massive objects and the faster evolution of massive stars Miller and Scalo (1979). Statistical studies of HAeBes are generally less reliable than those of TTS, as they are based not on complete samples from various star-forming regions but on small, disparate subsamples from the above-mentioned lists and assume different stellar and circumstellar characteristics.

An important step in the study was the use of parallax and magnitude data from the Gaia DR2 archive Lindegren et al. (2018). The work of Wichittanakom et al. (2020) not only updated most of the spectroscopically determined stellar masses, luminosities, surface gravities, and ages of southern HAeBe stars obtained by Fairlamb et al. (2015) using Gaia DR2 distances but also extended the same spectroscopic analysis to additional HAeBe stars in the north. Thus, the data from Wichittanakom et al. (2020) represent to date the most robust and homogeneous stellar characterization of a broad sample of HAeBe stars, including definitive spectroscopic data for 121 such stars, mostly based on Gaia DR2 distances.

Following these studies, it become clear that, based on certain characteristics, HAeBe stars are conditionally divided into two groups. HAe stars have lower mass (2–3 $M_\odot$) and greater ages ($t > 3$ Myr), while HBe stars have higher masses ($t > 3M_\odot$) and ages $t < 3$ Myr. The deficit of more massive older HBe stars is due to the more rapid evolution of stars toward the main sequence (MS). The paucity of very young HAe stars is likely due to two main reasons. First, HAe stars become optically visible later in their evolution, and second, the younger population of intermediate-mass T Tauri (IMTT) stars that evolve into HAe stars is not well studied.

To date, the formation and early evolution of massive stars has not been adequately studied. In their early stages, massive stars are hidden behind vast amounts of optical absorption. The significantly higher luminosity and intense ultraviolet radiation of young massive stars greatly influence their

* Contact e-mail: faidahuseynova@gmail.com

environment. Furthermore, the geometry and composition of the gas and dust around the star, as well as the dissipation time of this matter, may differ from those of low-mass stars. The existence of a strong stellar wind further complicates matters. The absence of a prolonged Pre-Main Sequence phase, during which circumstellar matter slowly dissipates and planetary systems can form, points to an important qualitative difference between massive and low-mass young stars. However, the maximum stellar mass required to form planetary systems is unknown.

This paper presents the results of spectral studies of Herbig Ae/Be stars with different masses, selected from the catalog of Guzmán-Díaz et al. (2021). Some physical characteristics of the program stars, collected from the scientific literature, are given in Table 1. The columns of Table 1 from left to right are object name, interstellar reddening coefficient A_V, distance D, stellar magnitude m_V, luminosity $L/L_\odot$, effective temperature $T_{\rm eff}$, radius $R/R_\odot$, mass $M/M_\odot$, age t, spectral class Sp type, equivalent emission width Hα EW(Hα), and reference to the relevant literature (Ref.).

2 OBSERVATIONS AND RESULTS

2.1 SPECTRAL OBSERVATIONS

Spectral observations of the program stars were carried out at the Cassegrain focus of the 2 m telescope of the Tusi Shamakhy Astrophysical Observatory (ShAO) using the Modified Universal Astro Grid Spectrograph (MUAGS). An Andor CCD camera (model iKon L-936-BEX2-DD) with 2048×2048 elements and a pixel size of 13.5 µm was used as the detector. To adapt the CCD to the spectrograph, a fast Canon EF lens ($f = 200$ mm, $f/2$) was installed in the spectrograph camera. The collimator has a focal length of 1100 mm, while the camera focal length is 200 mm. The angle of incidence α and diffraction angle β are 27.5° and 20.5°, respectively. The resolution in the camera focal plane is determined by the width of two pixels, giving a monochromatic slit image of $S' = 2\,\text{px} = 0.027$ mm for 1×1 binning. A diffraction grating with 651 lines/mm was used, which in first order with 1×1 binning provides a linear inverse dispersion of 144 Å/mm across the wavelength range of $\lambda = 3600-8000$ Å. In other words, in the region of the Hα line (λ6562.816 Å) in this mode, we have obtained a moderate spectral resolution of about $R = 3400$. A more detailed description of the spectrograph and the observation method is given in Ismailov et al. (2023).

The entire process of observation and data reduction was performed using the DECH program [1] (Galazutdinov, 2025). Table 2 presents the average UT time for the acquisition of two spectrograms per star. After calibration and processing, all spectra were averaged and normalized to the continuum.

Our spectral observations were executed during the period 2023 November 8–2024 August 9. Table 2 presents the observation log. The columns, from left to right, list the target name, observation date, exposure time, UT, binning, and signal-to-noise ratio (S/N) at the Hα line region in the spectrum. After calibration and processing, all spectra were averaged for the nights and normalized to the continuum. For the spectra of standard stars, the standard deviation in measurements for the radial velocities (R_V) of strong lines is ±5 km/s, and for the equivalent widths (EW) of hydrogen lines for A0–A6 type stars is ±0.5 Å.

Table 3 presents the results of measurements of individual spectral lines for the program stars. The absence of data for some lines indicates that, due to their weakness or absence in the spectrum, it was not possible to measure these lines from the spectra. For all stars, the Hα line is observed in emission. Some spectral features of individual stars are discussed in separate comments.

[1] http://www.gazinur.com/DECH-software.html

3 PHOTOMETRIC BVR$_C$I$_C$ OBSERVATIONS

Our photometric observations of the stars were carried out on the Zeiss-600 telescope using a BVR$_c$I$_c$ photometer, which is mounted at the Cassegrain focus of the telescope ($F = 7500$ mm) with a relative aperture $A = 1 : 12.5$. As a light detector, we used a FLI 4K×4K CCD camera with a pixel size of 9 μm. The useful field of the image frames was $17' \times 17'$. When applying binning 2×2 or 4×4, the resolution per pixel was 0.49"/px or 0.99"/px, respectively. The photometric data were obtained and processed using standard procedures of the MaximDL software package. A detailed description of the photometric system is given in Abdullaev et al. (2012). Transformation of our photometric system to the international standard was carried out in Ismailov and Valiev (2022).

Under the astroclimate conditions at ShAO, the seeing disk is typically 1.5–2". Under such conditions, components located at an angular distance of 3–4", as noted in Finkenzeller and Mundt (1984), will not be resolved with a 4×4 binning combination. In the obtained FITS frames, the stellar images did not deviate from a circular shape, and when measuring brightness, the object's image was completely covered by the chosen aperture size of the measuring circle. In this case, the aperture of the measuring circle was about 6". The average root-mean-square measurement error according to our data in individual bands was ±0.02 mag in V, ±0.008 mag in B, ±0.005 mag in R_c, and ±0.009 mag in I_c. Details of the photometric observation results are provided in the individual star comments.

4 COMMENTS ON INDIVIDUAL STARS

4.1 V1478 CYG

Three pairs of spectra were obtained in 2023 and two pairs in 2024. Figure 1 shows sections of the star's spectrograms in different wavelength intervals. The strongest identified lines

Table 1. Physical characteristics of program stars collected from the literature

Target	A_V	D (pc)	$L/L_\odot$	$T_{\rm eff}$ (K)	$R/R_\odot$	$M/M_\odot$	t (Myr)	Sp. type	EW(Hα)	Ref
MWC 1051	2.84	4530	4.03	20000	9	10.8	0.08		−157.7	11
	4.00									16
	4.84									15
	1.01				4	10.59				2
		2500								13
						16.08	0.04	B0pb		14
MWC 1080	5.40									1
	8.24			31500						5
	5.30	1000								9
		1000								4
	5.30	1000			7	20.6				13
	8.24		6.53			> 6	< 0.01			8
	1.67									15
AS 470		4040				7	0.1		−49.2	14
	2.27		3.01	8200						10
		700				9.36	0.1	B1Ia+e		3
MWC 300						9.36	0.1	B1Ia+e		14
	4.23				3.33	7.37				2
MWC 1021		3650				32	0.01	Bpe		14
	8.80									16
V1478 Cyg	3.10									15
										14

References: (1) Cohen M., Kuhi L.V. 1979, ApJS, 41, 743; (2) Liu T., et al. 2011, ApJ, 734, 22; (3) Terranegra L., et al. 1994, A&AS, 104, 557; (4) Eisner J.A., et al. 2004, ApJ, 613, 1049; (5) Mathew B., et al. 2018, ApJ, 857, 30; (6) Mendigutía I., et al. 2011, A&A, 529, A34; (7) Verhoeff A.P., et al. 2012, A&A, 538, A101; (8) Manoj P., et al. 2006, ApJ, 653, 657; (9) Corcoran M., et al. 1997, Nature, 390, 587; (10) Vioque M., et al. 2018, A&A, 620, A128; (11) Vioque M., et al. 2022, ApJ, 930, 39; (12) Henning T., et al. 1994, A&A, 291, 546; (13) Hillenbrand L.A., et al. 1992, ApJ, 397, 613; (14) Thomas S., et al. 2023, AJ, 165, 135; (15) Chen P.S. 2016, New Astron., 44, 11; (16) Hou J.L., et al. 1997, A&A, 327, 725.

Table 2. Log of spectral observations of program stars

Target	Spectra	Date	UT	Exp (s)	S/N
V1478 Cyg	KUA1541–42	11.08.2023	21:21	1600	28
V1478 Cyg	KUA1600–01	13.08.2023	23:59	1500	24
V1478 Cyg	KUA1653–54	16.08.2023	00:05	1500	22
V1478 Cyg	KUA1713–14	06.06.2024	21:24	1800	13
V1478 Cyg	KUA1744–45	05.07.2024	17:59	3000	15
MWC 1051	KUA1577–78	12.08.2023	00:08	1500	31
MWC 1051	KUA1787–88	04.08.2024	17:43	3000	32
MWC 300	KUA1524–25	11.08.2023	18:36	2000	25
MWC 300	KUA1667–68	17.08.2023	19:55	1800	22
AS 470	KUA1546–47	11.08.2023	22:43	900	30
AS 470	KUA1754–55	09.07.2024	18:55	2700	26
AS 470	KUA1248–49	08.09.2024	18:56	2400	36
MWC 1080	KUA1817–18	06.08.2024	19:18	1200	93
MWC 1021	KUA1535–36	11.08.2023	20:22	600	109
MWC 1021	KUA1596–97	13.08.2023	22:48	900	105
MWC 1021	KUA1649–50	16.08.2023	23:08	1200	112

are marked. As can be seen, the star's spectrum exhibits pure emission features. The intensity level shows significant variability over time. The star's spectrum showed variability with characteristic timescales of months to years (Table 3). Almost all hydrogen lines (Hα–Hγ) and helium lines (He I 5876, 6678) showed significant variations in equivalent widths. Based on two brightness estimates, there is a brightness variability of about 0.2 mag in the V-band.

4.2 MWC 1051

Two pairs of spectrograms of the star were obtained at an interval of about one year. Figure 2 shows the spectrograms obtained in 2023 and 2024. The Hα line exhibits a two-component profile with a very strong red component. The Hβ, Hγ, and Hδ lines display P Cyg-type emission profiles with an invisible blue emission component. A deep absorption component is particularly noticeable in the Hβ line in the blue wing, shifted by −350 to −400 km/s. The central absorption in the Hα line is blueshifted by about 10 Å, equiva-

Table 3. The results of measurements equivalent widths of spectral lines

Target	JD 2450000+	EW(Hα) [Å]	EW(Hβ) [Å]	EW(Hγ) [Å]	EW(He I 5876) [Å]	EW(D Na I) [Å]	EW([O I] 6300) [Å]
V1478Cyg	60168.389	781.47	16.57	0.79	26.58		7.89
V1478Cyg	60170.499	1010.82	13.16	0.55	29.15		7.55
V1478Cyg	60172.503	1081.96	24.29	1.62	35.59		9.28
V1478Cyg	60468.391	365.45	43.45	5.45	46.81		12.04
V1478Cyg	60497.249	1000.30	32.26	2.42	38.61		9.20
MWC 300	60168.275	148.34	1.89	0.44	0.64		9.92
MWC 300	60174.329	128.28	0.99	6.18	0.42	1.7	8.80
MWC 1051	60168.505	142.34	10.53	0.58	0.63*	1.65	0.77
MWC 1051	60527.238	133.80	10.37	1.59	0.74*	1.7	1.46
AS 470	60168.446	45.26	3.79	0.46	0.92		1.94
AS 470	60501.288	46.46	3.58	0.58	0.80	2.77	3.00
AS 470	60562.289	34.53	2.67	0.26	0.80	3.44	
MWC 1080	60529.304	42.62	2.79	0.68		1.01	
MWC 1021	60168.344	236.10	11.63	0.67	1.59		0.35
MWC 1021	60170.450	138.77	2.03	0.11	1.701		0.10
MWC 1021	60173.460	199.23	7.97	0.39	1.09		0.23

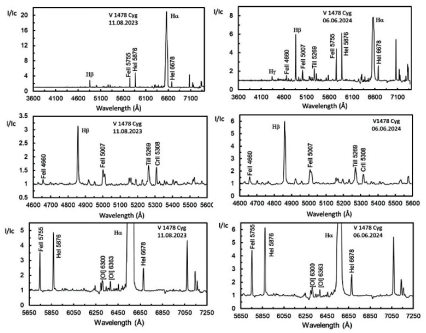

Figure 1. Comparison of continuum-normalized spectrograms of V1478 Cyg from 2023 and 2024. Top panels show the full spectral range, middle panels show the λ4600–5600 Å region, and bottom panels show the λ5650–7250 Å region

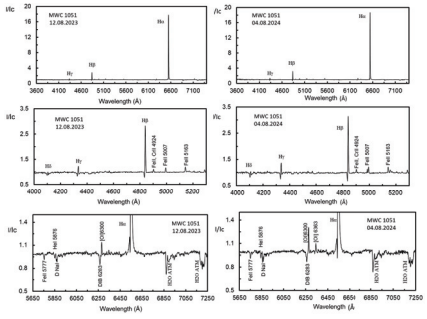

Figure 2. The same as in Fig. 1 for the star MWC 1051

lent to a velocity of approximately −450 km/s. This indicates that the star possesses a significant stellar wind and disk accretion. The He I 5876 and D lines of Na I are observed in absorption. The forbidden doublet [O I] $\lambda\lambda$6300, 6363, as well as the interstellar absorption band DIB 6283, are clearly visible, indicating a complex circumstellar structure in the star's disk. A comparison reveals that in 2024 the star exhibits a more developed emission spectrum than in 2023.

4.3 MWC 300

The star MWC 300 exhibits properties of B[e] stars. Studies by different authors provide conflicting histories of its exploration. Merill and Bowen (1951) classified the star as intermediate between ordinary Be stars and planetary nebulae. Herbig and Rao (1972) included the star in their catalog, while Finkenzeller and Mundt (1984) noted that the object probably does not belong to young stars. Allen Swings (1976) classified the star's spectrum as Bep. Appenzeller (1977) was the first to note the rich photospheric spectrum, which agrees well with the spectrum of B1 Ia. This conclusion was confirmed by Wolf Stahl (1985).

Miroshnichenko et al. (2004) conducted extensive spectroscopic and photometric studies of MWC 300 and strengthened the case for classifying it as a supergiant with an effective temperature of 19,000 K, a distance of 1.8 ± 0.2 kpc, and a luminosity of $\log L/L_{\odot} = 5.1 \pm 0.1$.

In spectroscopic observations by Corporon and Lagrange (1999) and Miroshnichenko et al. (2004), and astrometric measurements by Takami et al. (2003), the star shows signs of binarity.

On August 11 and 17, 2023, we obtained two pairs of spectrograms of the star. The measured equivalent widths on August 11, 2023, are approximately 50% larger than those on August 17, 2023. Fragments of the star's spectrum are shown in Fig. 3. Over the course of our six days of observations, noticeable changes in the intensity of emission lines in the star's spectrum were detected.

4.4 AS 470

We obtained three spectra of the star on August 11, 2023, July 9 and September 8, 2024. Figure 4 shows fragments of the star's spectrum obtained at intervals of one year. On

Table 4. Results of photometrical observations of some program stars.

Target	Date	JD (245+)	I_c	B	V	R
MWC 300	24.07.2023	60149.306	12.644	12.201	11.956	11.982
MWC 300	28–29.07.2023	60154.225			11.842	11.808
MWC 300	08–09.08.2023	60165.260	12.500		11.537	12.036
MWC 300	15–16.08.2023	60172.332	12.640		11.808	11.604
MWC 1080	23–24.08.2023	60180.356	9.842	12.480	11.559	10.674
V1478 Cyg	06–07.08.2023	60163.296	12.670	12.921	13.220	12.375
V1478 Cyg	21–22.08.2023	60178.293			13.038	12.352
AS 470	15–16.08.2023	60172.386	14.660	12.010	12.760	13.802
AS 470	16–17.08.2023	60173.352	13.907	11.421	12.761	13.800
AS 470	21–22.08.2023	60178.358	14.71	11.209	12.778	13.844

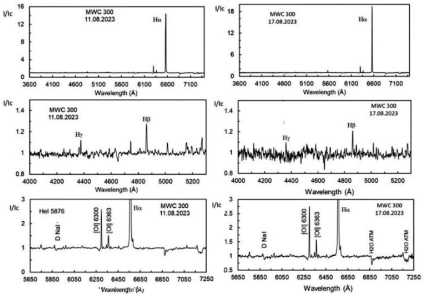

Figure 3. The same as in Fig. 1 for the star MWC 300

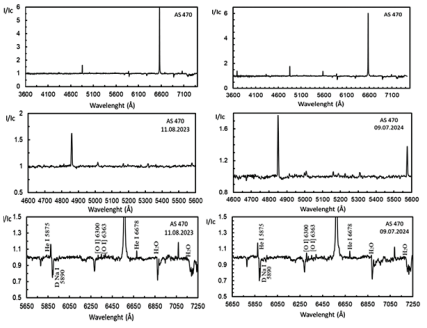

Figure 4. Normalized spectra of the star AS 470 for the dates 11.08.2023 and 09.07.2024 are shown. The panels below show a larger-scale representation of the spectrum on those dates in the region of λ 4600–5600 Å, and λ 5650–7250 Å

August 11, the intensities of the emission lines in the spectrum noticeably weakened. During the observation period, the equivalent width of the Hα emission line changed from 46 to 34 Å, which is consistent with the data from Guzmán-Díaz et al. (2021). Our photometric observations, conducted on three dates during August 15–22, 2023, revealed brightness variations in the B and V bands with amplitudes of 0.8 mag and 0.7 mag, respectively. In the red bands, the brightness change is insignificant.

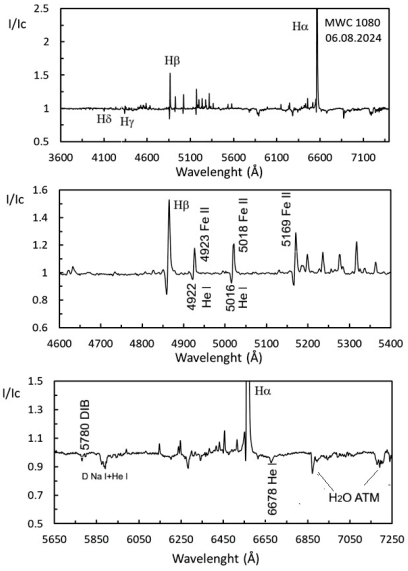

Figure 5. The same as in Fig. 1 for the star MWC 1080

4.5 MWC 1080

For the first time, Shevchenko et al. (1994) found a photometric period of about 2.9 days and Corporon and Lagrange (1999) confirmed spectroscopic binarity with this period. We obtained only one pair of spectra of the star, which were averaged. Figure 5 shows fragments of the resulting spectrum of the star. In addition to strong hydrogen emission lines, the star's spectrum contains deep absorption lines of He I, lines of the interstellar band DIB 5780, and many lines of ionized iron. The hydrogen lines exhibit typical P Cygni profiles, indicating a strong outflow of matter. The Balmer decrement is steep (see Table 3), indicating a large optical depth of the envelope. The spectral type of the star corresponds to early B0–B1 Ve.

4.6 MWC 1021

According to the data from the catalog of Guzmán-Díaz et al. (2021), the distance to the star is more than 3090 pc, spectral

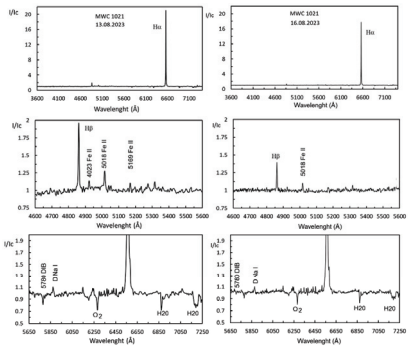

Figure 6. The same as in Fig. 1 for the star MWC 1021

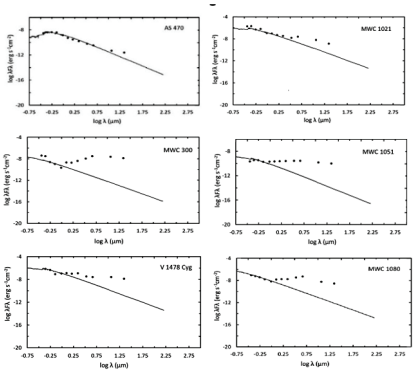

Figure 7. Spectral energy distribution (SED) curves for program stars. The solid line represents the model SED from Castelli and Kurucz (2004)

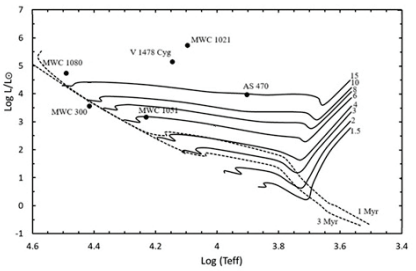

Figure 8. Theoretical HR diagram according to Bressan et al. (2012) for program stars. The solid curves represent evolutionary tracks labeled with masses (in $M_\odot$), and the dashed curves represent isochrones for ages of 1 and 3 Myr

class B6–B7, radius $R/R_\odot \sim 154$, luminosity $L/L_\odot \sim 5.8$, age $t < 0.01$(Myr), and mass $M/M_\odot \sim 73.6$. We obtained three pairs of spectra of the star in 2023. As can be seen from Table 3, the equivalent widths of the emission lines are significantly larger in 2023. Figure 6 shows fragments of the spectrum of MWC 1021, obtained on two different nights. As can be seen, the star's spectrum is characterized by emission lines of hydrogen, ionized iron, and the 5780 Å DIB line of interstellar origin. A comparison revealed that over the four nights of observations between August 13 and 16, the star's emission spectrum showed a significant decrease in the equivalent widths of hydrogen and ionized iron emission lines.

5 SPECTRAL ENERGY DISTRIBUTION (SED) IN THE SPECTRUM AND PHYSICAL PARAMETERS OF STARS

Using data from Vizier catalogues and following the method described in Adigozalzade et al. (2025), we constructed spectral energy distribution (SED) curves for the program stars. Figure 7 shows the energy distribution curves of the program stars in the range 0.36–22.1 μm. Observational data were taken from the 2MASS and WISE catalogs and transformed into absolute fluxes, taking into account interstellar reddening (see Ismailov and Valiev 2022). Data from the IRAS catalog are not available for these stars, so values from the WISE catalog were used in the far-IR region.

As can be seen from Fig. 7, individual stars show a complex distribution, which is poorly approximated by the model SED curve taken from Castelli and Kurucz (2004). The type of SED curves is determined from the magnitude of the IR excess emission. The star AS 470 shows a weak excess emission of cool dust, starting at 11.6 μm. This suggests that the disk of the star consists primarily of residual dust. The remaining stars show both gas and dust excesses in their disks. The stars AS 470 and MWC 1021 exhibit type III SED curves, the stars V1478 Cyg and MWC 1051 show type II, and MWC 300 and MWC 1080 belong to type I according to the classification of Lada (1987).

Knowing the value of interstellar extinction A_V, the refined distance to the star D according to Gaia data, the stellar magnitude V, and the bolometric correction m_b Pecaut and Mamajek (2013), the luminosity, radius, and absolute magnitude of the program stars were calculated using standard expressions. The effective temperature of the star corresponding to its spectral class according to Pecaut and Mamajek (2013) was used. The effective temperature and bolometric luminosity of the Sun were also used in the calculations. Table 5 shows the obtained parameters of individual stars, as well as the types of SED curves according to Lada (1987).

Figure 8 shows the theoretical HR diagram according to Bressan et al. (2012). The dots indicate the positions of the program stars. From this diagram, the masses and ages of the stars under study were determined. These parameters are also given in Table 5.

6 DISCUSSION AND CONCLUSIONS

As is known, the formation of circumstellar disks is a natural outcome of star formation, since a young protostar, forming from a parent molecular cloud, must preserve its initial angu-

Table 5. Physical parameters of the program stars

Object	V	A_V	D (pc)	M_V	BC	$\log(L/L_\odot)$	$\log T$	$R/R_\odot$	$M/M_\odot$	t (Myr)	SED
MWC 1051	12.837	0.9	4873	−3.1	−1.58	3.16	4.23	13.044	6	0.8	II
V1478 Cyg	13.15	9	1669	−8.0	−1.07	5.14	4.15	154.795	25	0.2	II
MWC 300	13.795	4	1786	−4.1	−2.61	3.56	4.41	13.469	9	3	I
AS 470	11.72	2.5	7278	−5.1	−0.02	3.98	3.90	70.5261	15	0.3	III
MWC 1080	11.859	5	1489	−7.0	−3.03	4.75	4.49	44.1734	20	0.5	I
MWC 1021	13.08	9	3649	−9.5	−0.79	5.74	4.10	344.106	35	0.1	III

lar momentum during compression. Ring-shaped dust structures have been discovered in disks around low-mass protostars, which may be remnants of early dust evolution (see, for example, Mamedkhanova and Ismailov (2019) and citations therein). Circumstellar disks likely facilitate the subsequent formation of planetary systems around stars. Therefore, circumstellar disks play a crucial role in the formation of stars and planets.

Our data showed that all program stars exhibit significant variability in their disk emission. This is reflected in the variability of the hydrogen emission lines of the Balmer series, the He I 5876 lines, and the doublet D Na I. Individual photometric observations indicate significant variability in the brightness of program stars. Theoretical work shows that non-stationarity in the disks of massive young stars is a completely expected real process that can arise due to the accretion of matter into the outer parts of the disk and the radiation of a high-temperature central source (see, for example, Zhao et al. (2020)).

As can be seen from Table 5, despite their young ages, two of the most massive stars, AS 470 and MWC 1021, are close to complete dissipation of their circumstellar disks. Their excess disk emission begins at $\lambda \geqslant 10\ \mu$m. As shown in Adigozalzade et al. (2025) such stars have a residual dust disk that has virtually lost its gas component. Most often, these stars have type III SED curves according to the classification of Lada (1987). Similar residual disks have been observed, for example, in Vega-type stars (see, Ismailov et al. 2021). This shows that, despite their still young ages, two of the objects, AS 470 and MWC 1021, are already close to the end of the disk dissipation stage and have lost their gas component. Due to the large mass of the central star, their disk evolution was relatively rapid.

Thus, of the six program young massive stars, two have a debris disk, two have an intermediate disk, and one has strong disk emission. The characteristics of the star MWC 300 indicate that its IR excess emission may be due to the presence of a secondary component. The star is an interesting object that has characteristics of B[e] stars (see, for example, Miroshnichenko et al. (2004)). From Fig. 8 it is evident that the star MWC 300 has already reached the Main Sequence, and despite this, it still has powerful IR emission. Rather, the additional emission in the star's SED is an argument in favor of its binarity Takami et al. (2003); Wang et al. (2012) and the emission in forbidden lines is formed in the circumstellar gas ring.

(i) All program stars show variations in their emission spectrum and brightness. Disk activity in massive stars may be the result of accretion in the outer part of the disk and high-temperature radiation from the central star.

(ii) The weak excess IR emission from AS 470 and MWC 1021 indicates that the circumstellar disks of these stars have lost their gas component and have weak dust emission, which is also characteristic of Vega-type stars.

(iii) Despite its young age, MWC 300 has already reached the main sequence in its physical parameters. Despite this, the star possesses powerful disk radiation, which is rather formed within the ring-shaped circumstellar envelope.

REFERENCES

Abdullaev B.I., Alekberov I.A., Gyulmaliev N.I., et al., 2012, Azerbaijani Astronomical Journal, **7**, 39

Adigozalzade H.N., Ismailov N.Z., Valiyev U.S., Huseynova F.S. et al., 2025, Advances in Space Research, **76**, 1854

Allen D.A., Swings J.P., 1976 Astrophysical Journal, **47**, 293

Appenzeller, I., 1977, Astronomy & Astrophysics, **61**, 21

Bo Zhao, Tomida K., Hennebelle P., et al., 2020 Space Science Reviews, **216**, 43

Bressan A., Marigo P., Girardi L. et al., 2012 Monthly Notices of the Royal Astronomical Society, **427**, 127

Carmona A., van den Ancker M.E., Audard M. et al., 2010, Astronomy & Astrophysics, **517**, A67

Castelli F., Kurucz R.I., ATLAS9, 2004

Chen P.S., Shan H.G., Zhang P., 2016, New Astronomy, **44**, 1

Corporon P., Lagrange A.M., 1999, Astronomy & Astrophysics Supplement Series, **136**, 429

Fairlamb J.R., Oudmaijer R.D., Mendigutía I., Ilee J.D., van den Ancker M.E., 2015, Monthly Notices of the Royal Astronomical Society, **453**, 976

Finkenzeller U., Mundt R., 1984, Astronomy & Astrophysics Supplement Series, **55**, 109

Guzmán-Díaz J., Mendigutía I., Montesinos B., et al., 2021, Astronomy & Astrophysics, **650**, 182

Herbig, G.H., and Bell, K.R., 1988, Third Catalog of Emission-Line Stars of the Orion Population: 3: 1988

Herbig, G.H., 1960, Astrophysical Journal Supplement Series, **4**, 337

Herbig, G.H., Rao, N.K., 1972, Astrophysical Journal, **174**, 401

Ismailov N.Z., Alyshov S.A., Ismailova Sh.K., Huseynova F.S., 2023, Astronomy Reports, **67**, 1056

Ismailov N.Z., Kholtygin A.F., Romanyuk I.I., Pogodin M.A., Moiseeva A.V., 2021 Astrophysical Bulletin, **76**, 415

Ismailov N.Z., Valiev U.S., 2022 Astronomy Reports, **66**, 965

Lada C.J., Proceedings of the Symposium, Tokyo, Japan, Nov. 11-15, 1985 (A87-45601 20-90)/IAU Symposium, Tokyo: 1987. **115**, 1

Lindegren L., Hernández J., Bombrun A. et al., 2018, Astronomy & Astrophysics, **616**, A2

Mamedkhanova, G.B., Ismailov, N.Z., 2019, Astronomy Reports, **63**, 190.

Merill P.W., Bowen I.S., 1951, Publications of the Astronomical Society of the Pacific, **63**, 295.
Miller, G., and Scalo, J., 1979, Astrophysical Journal Supplement Series, **41**, 513.
Miroshnichenko A.S., Levato H., Bjorkman K.S., et al.,2004, Astronomy & Astrophysics, **417**, 731.
Pecaut, M.J., Mamajek, E.E., 2013, Astrophysical Journal, Supplement Series, **208**, 9.
Shevchenko V.S., Grankin K.A., Ibragimov M.B. et al., 1994, van den Heuvel EPJ (eds.), **62**, 43.
Takami M., Bailey J., Chrysostomou A., 2003, Astronomy & Astrophysics, **397**, 675.
The P.S., de Winter D., Perez M.R., 1994, Astronomy & Astrophysics Supplement Series, **104**, 315.
Valiyev U.S., Alishov S.S., Ismailov N.Z., 2022, Peremennye Zvezdy, **42**, 51.
Wang Y., Weigelt G., Kreplin A., et al., 2012, Astronomy & Astrophysics, **545**, L10.
Wichittanakom C., Oudmaijer R.D., Fairlamb J.R. et al., 2020, Monthly Notices of the Royal Astronomical Society, **493**, 234.
Wolf B., Stahl O., 1985, Astronomy & Astrophysics, **148**, 412.